Full Paper

Journal of the Brazilian Chemical Society

https://dx.doi.org/10.21577/0103-5053.20250130

J. Braz. Chem. Soc. **2025**, *36*, 12, e-20250130, 1-13

LIBS and Hyperspectral Imaging as a Real-Time Process Control Tool for Metal Recovery from E-Waste

Dennis S. Ferreira[a] *and Edenir R. Pereira-Filho*[*,a]

[a]*Departamento de Química, Universidade Federal de São Carlos, 13565-905 São Carlos-SP, Brazil*

The rapid increase in e-waste creates challenges, requiring more efficient recycling methods. This study explores the application of laser-induced breakdown spectroscopy (LIBS) combined with hyperspectral imaging to monitor leaching processes of Ag, Au, Cu and Sn in e-waste recycling. The method involved the use of sequential leaching strategies of printed circuit boards (PCBs), the best strategy was applied using HNO_3 for Cu, HCl for Sn and thiourea/$Fe(NO_3)_3$ for Ag and Au. Inductively coupled plasma optical emission spectrometry (ICP OES) was used to validate the metal extraction efficiency, achieving recoveries of 100% for Cu and Ag, 97% for Sn and 86% for Au. LIBS spectra showed a strong correlation with the ICP OES data, revealing reductions in the emission signals corresponding to the extracted elements. Hyperspectral imaging provided an analysis of the spatial distribution of trace elements, confirming the progressive extraction of metals. The results indicate that LIBS, associated with multivariate analysis, offers a fast and economical alternative.

Keywords: e-waste recycling, LIBS, hyperspectral imaging, sustainable recovery, ICP OES, circular economy

Introduction

The rapid technological advancement and increasing demand for electronic equipment have led to an exponential growth in electronic waste (e-waste) generation. This issue is exacerbated by planned obsolescence, particularly in small electronic devices such as smartphones and tablets, which often have lifespans of only 2-3 years.[1,2] In 2022, an estimated 62 million metric tons (Mt) of e-waste were generated globally, and projections indicate this could surpass 110 Mt by 2050.[3] Alarmingly, only 22.3% of this waste is formally recycled, while a large portion is either processed informally or improperly discarded in landfills, leading to environmental and health risks.[4,5]

Informal recycling is frequently carried out under unsafe conditions, releasing hazardous substances such as polychlorinated dibenzofurans (PCDFs) and dioxins. These persistent organic pollutants (POPs), mainly associated with the non-metallic fraction of e-waste, represent significant risks to human health and ecosystems.[6] In this context, the implementation of safe, scalable, and sustainable recycling practices is urgently needed to support environmental regulations such as the Stockholm Convention.[7,8]

Hydrometallurgical methods have emerged as an environmentally friendly alternative to pyrometallurgy for metal recovery from printed circuit boards (PCBs). These processes are cost-effective, adaptable, and operate under milder conditions than pyrometallurgical routes.[9] Pyrometallurgy requires energy-intensive furnaces operating at temperatures typically exceeding 1200 °C, a condition known to promote the formation of hazardous byproducts such as polychlorinated and polybrominated dibenzofurans (PCDFs/PBDFs) and dioxins from the combustion of the plastic and flame-retardant fraction of the e-waste.[10,11]

In contrast, hydrometallurgical leaching operates at or near atmospheric pressure and at significantly lower temperatures, generally below 100 °C and often at room temperature, as employed in this study.[12,13] This fundamental difference not only reduces energy consumption but, critically, prevents the formation of the previously mentioned thermogenic persistent organic pollutants (POPs), shifting the environmental challenge from air emissions to the management of aqueous effluents.[14]

Among the stages involved leaching, separation, and purification leaching plays a critical role, as it directly determines the efficiency of metal recovery.[15,16] However, challenges remain regarding extraction selectivity, operational control, and scalability, particularly in

*e-mail: erpf@ufscar.br
Editor handled this article: Josué Carinhanha Caldas Santos (Associate)

multi-element systems containing both base and precious metals such as Cu, Ag, Au, and Sn.[17,18]

Process monitoring is essential for optimizing leaching efficiency, minimizing chemical consumption, and reducing environmental impact. Conventional techniques such as inductively coupled plasma optical emission spectrometry (ICP OES) and X-ray fluorescence (XRF) are reliable but limited by high costs, complex sample preparation, and the need for laboratory infrastructure.[19,20] In contrast, optical spectroscopic techniques especially laser-induced breakdown spectroscopy (LIBS) offer a promising alternative for real-time, *in situ* analysis. LIBS is fast, versatile, requires minimal sample preparation, and can be combined with chemometric tools such as Principal Component Analysis (PCA) or Partial Least Squares (PLS) to extract meaningful insights from complex data sets.[21-23]

However, the feasibility and optimization of these processes on an industrial scale are fundamentally limited by an analytical difficulty: the absence of process technology capable of monitoring the solid phase in real-time. The reliance on *ex situ* laboratory analyses, such as ICP OES, hinders dynamic and fast control of the process, resulting in non-optimized residence times and excessive reagent consumption.[24,25]

This research is therefore justified by the critical need to overcome this limitation. The aim is to validate a method that integrates the speed of LIBS analysis with the spatial resolution of hyperspectral imaging, establishing a robust tool for directly monitoring the concentration reduction of metals in the solid matrix. We thus aim to provide the missing analytical link to enable intelligent control and real-time optimization of hydrometallurgical processes applied to complex wastes.

Experimental

Instrumentation

Laser-induced breakdown spectroscopy (LIBS)

The LIBS spectra were obtained using the LIBS J200 instrument (Applied Spectra, Fremont, CA, USA), controlled by the Axiom 2.5 software (Applied Spectra), which is responsible for configuring the operating parameters. The equipment consists of an Nd:YAG laser (Quantel Ultra, Bozeman, MT, USA) with a wavelength of 1064 nm, a laser pulse duration of 5 ns and a maximum energy of 100 mJ *per* pulse, as well as a 6-channel charge-coupled device (CCD) spectrometer that records spectral information in the 186 to 1042 nm range. The spectral ranges and resolutions of each spectrometer channel are as follows: 186-311 nm (0.059 nm), 311-465 nm (0.073 nm), 465-591 nm (0.062 nm), 591-693 nm (0.050 nm), 693-884 nm (0.094 nm) and 884-1042 nm (0.079 nm).

The adjustable operating parameters include the laser pulse energy, which varies from 0 to 100 mJ, the delay time, which corresponds to the interval between the emission of the laser pulse and the start of recording by the spectrometer, and can vary from 0 to 2 μs, and the spot size, which represents the diameter of the laser beam, adjustable between 50 and 250 μm. The sample is moved with the aid of a programmable XYZ stage, integrated with an image capture system consisting of a CMOS (complementary metal-oxide-semiconductor) color camera with a resolution of 1280 × 1024 pixels, allowing precise visualization and alignment. In addition, Aurora software version Rev 2.0 (Applied Spectra, Fremont, CA, USA) was used to identify the characteristic emission lines of each chemical element present in the spectra obtained.

Inductively coupled plasma optical emission spectrometry (ICP OES)

Reference or confirmatory values for the elements Ag, Au, Cu and Sn were obtained using the iCAP 7000 Series ICP OES instrument (Thermo Fisher Scientific, Waltham, MA, USA), operated under robust conditions, with axial and radial observations mode. All measurements were carried out using high purity argon gas (Ar) (99.999%, White Martins-Praxair). The instrumental conditions followed the recommendations of the manufacturer, with the radio frequency (RF) power set at 1.15 kW, the plasma flow rate at 12.0 L min^{-1}, the auxiliary flow rate at 0.50 L min^{-1}, and the nebulizer flow rate at 0.70 L min^{-1}. The integration time varied between 5 and 15 s, and a Mira Mist nebulizer and a cyclonic spray chamber were used. The emission lines monitored for the elements were: Ag (I 328.068 nm), Au (I 267.595 nm), Cu (I 327.296 nm) and Sn (I 283.999 nm). The limits of detection (LOD) were estimated according to the methods recommended by International Union of Pure and Applied Chemistry (IUPAC),[26] giving the following values: Ag (0.001 mg kg^{-1}), Au (0.004 mg kg^{-1}), Cu (0.006 mg kg^{-1}) and Sn (0.04 mg kg^{-1}).

Reagents and standard solutions

All the solutions used in this study were prepared with ultrapure water produced in a Milli-Q® Plus system (Millipore Corp., Bedford, MA, USA). Before use, all the glassware and polypropylene bottles were decontaminated with detergent, immersed for 24 h in a solution of nitric acid (HNO_3 10% v v^{-1}) (Synth, Diadema, Brazil) and then rinsed with ultrapure water. The external calibration curves for the elements Au, Ag, Cu and Sn were drawn up by

successive and appropriate dilutions of a standard stock solution of 1000 mg L^{-1} (Specsol, São Paulo, Brazil) using HNO_3 solution. The reagents used in the leaching processes included: HNO_3, H_2SO_4 (Synth, Diadema, Brazil), HCl (Química Moderna, Barueri, Brazil), I_2 (Grupo Química, Penha, Brazil), KI (Synth, Diadema, Brazil), thiourea (Neon, Suzano, Brazil), $Fe(NO_3)_3$ (Synth, Diadema, Brazil) and $CuSO_4$ (Synth, Diadema, Brazil). The concentrated acids HNO_3 and HCl were previously purified by distillation using the Distillacid™ BSB-939-IR system (Berghof, Eningen, Germany).

Sampling, preparation and characterization of samples

The material utilized in this study was a 1.2 kg composite powder of PCBs. This composite was prepared from PCBs recovered from various end-of-life (EoL) electronic equipment, with the following mass distribution: computers (56.7%), laptops (34.4%), tablets (4.8%), and cellphones (4.1%). To obtain the final analytical sample, these collected PCBs were first processed in a knife mill (Tecnal TE-650, Piracicaba, Brazil). The resulting powder was then thoroughly homogenized and subsequently sieved to isolate a standardized particle sizes fraction of less than 212 µm. This final, homogeneous powder served as the starting material for all characterization, leaching, and LIBS experiments.

The method adapted from Ferreira *et al.*[27] was used to characterize the samples. In this procedure, 100 mg of ground PCB sample was weighed and transferred to closed tetrafluoroethylene-perfluoro (alkoxy vinyl ether) vials (Savillex, 50 mL PFA block digestion tube, model 210-050-70). A mixture of 50% v v^{-1} aqua regia was then added, the tubes were closed and the system was heated to 100 °C in a model MA4025 digestion block (Marconi, Piracicaba, SP, Brazil) for 2 h. After cooling, the resulting solution from the digestion was filtered through filter paper and diluted to the appropriate concentration range using deionized water. The concentrations of Au, Ag, Cu and Sn present in the digested solution were determined by ICP OES, with all analyses carried out in triplicate and the results expressed as averages. All the steps mentioned are depicted in Figure S1 (see the Supplementary Information (SI) section).

E-waste leaching procedure

Sequential leaching was designed to maximize the selective extraction of Cu, Sn, Ag, and Au from PCB samples. The conditions for each step including the choice of leaching agent, temperature, and acid concentration were adapted from optimized literature methods, with each set of parameters tailored to maximize the dissolution of a specific metal while minimizing the co-extraction of others. The underlying principle is to use different chemical environments (oxidizing acids, complexing agents) to sequentially target base metals (Cu for instance) and, subsequently, the more inert precious metals (Ag and Au).

After each leaching step, both the solid and liquid fractions were separated, quantified, and stored for subsequent analysis (Figure 1). The solid residue was prepared for analysis according to the method adapted by Ferreira *et al.*[27] During all the leaching procedures, blank samples were processed simultaneously, in triplicate (n = 3).

Leaching Cu with HNO_3

For the leaching of Cu from the samples, 150 g of PCB were weighed and divided into 15 parallel sub-samples of

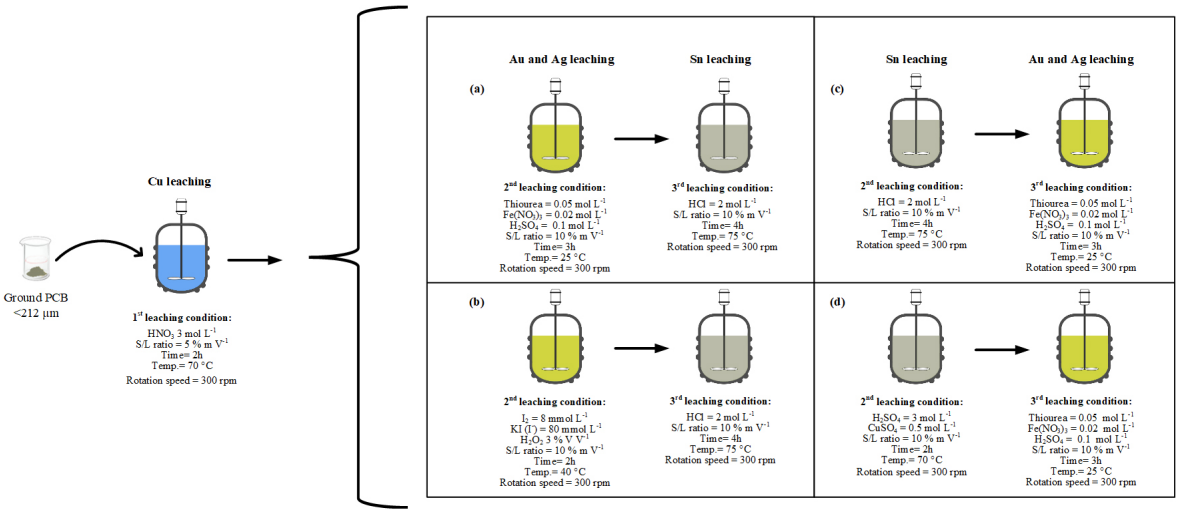

Figure 1. Sequential leaching tests for the extraction of Ag, Au, Cu and Sn from e-waste. (a) Acid leaching using thiourea with $Fe(NO_3)_3$; (b) leaching with iodine/iodide; (c) leaching with HCl; (d) leaching with H_2SO_4 and $CuSO_4$.

10 g each. The sub-samples were transferred to a 500 mL beaker and 200 mL of a 3 mol L^{-1} HNO_3 solution was added.

The HNO_3 was selected as a strong oxidizing agent capable of efficiently dissolving Cu, the primary metallic component, thereby simplifying the matrix for subsequent precious metal recovery. The mixture was stirred in a heated magnetic stirrer (model 752A, Fisatom, São Paulo, Brazil) at 300 rpm for 2 h at a temperature of 70 °C. This procedure adopted experimental conditions based on the parameters optimized by Dutta *et al*.[28] After the leaching stage, the solid and liquid phases were separated using quantitative filter paper (Unifil, black tape, 125 mm diameter, Germany).

The filtered sub-samples were combined and homogenized. The leached liquid was analyzed by ICP OES to determine the concentrations of Ag, Au, Cu, and Sn. The remaining solid residue was washed with deionized water and characterized according to the method described in the previous section, to evaluate the residual concentrations of the elements in the solid. A fraction of this solid residue was stored for subsequent leaching steps and LIBS analysis.

Leaching of Ag and Au

Acid leaching using thiourea with $Fe(NO_3)_3$

The leaching process was carried out to extract Ag and Au. Five g of the solid residue that was already submitted to Cu extraction, was weighed and mixed with 50 mL of a solution containing 0.05 mol L^{-1} of thiourea, 0.02 mol L^{-1} of $Fe(NO_3)_3$ as an oxidizing agent and 0.1 mol L^{-1} of H_2SO_4 (Figure 1a).

This step utilizes thiourea, a well-established complexing agent, which in the presence of an oxidant (Fe^{3+}) forms stable aqueous complexes with Au and Ag, enabling their extraction under mild acidic conditions. The solution was prepared in a 150 mL beaker, which was then placed on a magnetic stirrer. The mixture was stirred for 3 h at a constant speed of 300 rpm at room temperature. The experimental conditions adopted followed the parameters optimized by Behnamfard *et al*.[29] After leaching, the mixture was filtered to separate the solid and liquid phases. The extracts obtained were properly prepared and the concentrations of the target elements (Ag and Au) were determined using ICP OES. A fraction of this solid residue was stored for the next leaching and LIBS analysis.

Leaching with iodine/iodide

For this leaching process, 5 g of the solid residue was weighed and mixed with 50 mL of a solution consisting of 8 mmol L^{-1} of iodine, 80 mmol L^{-1} of iodide, and H_2O_2 (3%) as an oxidizing agent. The mixture was prepared in a 150 mL beaker and stirred on a magnetic stirrer at a constant speed of 300 rpm for 2 h at 40 °C (Figure 1b). The experimental conditions were adapted based on the parameters previously optimized by Xiu *et al*.[30] After the leaching stage, the mixture was filtered to separate the solid and liquid phases. The liquid and solid extracts were properly prepared, and the target elements were determined using ICP OES. A fraction of this solid residue was stored for the next leaching and LIBS analysis.

Leaching of Sn

Leaching with HCl

The leaching process was carried out to extract Sn in an acidic medium containing HCl. Specifically, 5 g of the solid residue was weighed and combined with 50 mL of a 2 mol L^{-1} HCl leaching solution (Figure 1c). The HCl was employed because the Cl^- effectively form stable aqueous complexes with Sn, promoting its dissolution at elevated temperatures.

The mixture was transferred to a 150 mL beaker and subjected to magnetic stirring for 4 h at a controlled temperature of 75 °C. The experimental conditions were adapted from the optimized parameters established by Moosakazemi *et al*.[31] Following the leaching procedure, the mixture was filtered to separate the solid and liquid phases. The resulting filtrates were subsequently prepared and analyzed to determine the concentrations of the target elements using ICP OES. A fraction of this solid residue was stored for the next leaching and LIBS analysis.

Leaching with H_2SO_4 and $CuSO_4$

For the acid leaching process with H_2SO_4, 5 g of the solid residue was weighed and mixed with 50 mL of a solution containing 3 mol L^{-1} of H_2SO_4 and 0.5 mol L^{-1} of $CuSO_4$. The mixture was prepared in a 150 mL beaker and stirred on a magnetic stirrer at a constant speed of 300 rpm for 2 h at a temperature of 70 °C (Figure 1d). The experimental conditions were adapted based on the parameters previously optimized by Guo *et al*.[32] After leaching, the mixture was filtered to separate the solid and liquid phases. The resulting extracts were prepared and analyzed, with a focus on determining the target elements by ICP OES. A fraction of this solid residue was stored for the next leaching and LIBS analysis.

LIBS data as an alternative process control in e-waste recycling

To prepare the samples for LIBS analysis, the solid residues were previously homogenized manually after each leaching process. Approximately 500 mg of each sample were weighed and pressed in a hydraulic press

model SSP-10 (Shimadzu, São Paulo, SP, Brazil) with a force of 60 kN, for 1 min, to form pellets with a diameter of 12 mm and a thickness of 2 mm, to optimize data acquisition by the instrument. All pellets were prepared in triplicate (n = 3).

The operating parameters used to acquire the spectra included laser pulse fluence of 1000 J cm^{-2}, spot size of 100 μm, a delay time of 1 μs, and laser pulse energy of 80 mJ. These parameters were selected based on previously established optimized conditions. After adjusting the parameters, the samples were placed in the ablation chamber in triplicate, and the laser focus was adjusted. The spectra acquisition pattern followed a 12 × 12 points arrangement, with 5 pulses applied to each point. The spectral data obtained generated a matrix with a dimension of 720 × 12,288, where 720 represents the total number of pulses (spectral signals = 12 × 12 × 5 = 720) recorded in the sample and 12,288 corresponds to the number of emission lines detected in the spectral range from 186 to 1,042 nm. All the steps of the LIBS analysis are illustrated in Figure S2 (see SI section).

Data processing and chemometric analysis

Raw spectral data from the LIBS analysis were initially organized using Microsoft Excel (Microsoft Corp., Redmond, WA, USA) and subsequently processed in MATLAB (R2019b, The MathWorks, USA). Due to the zigzag acquisition pattern intrinsic to the J200 LIBS system, a custom routine named LIBS_inverse developed by Ferreira *et al*.[33] was used to standardize the spatial order of the spectra into a linear format from left to right, enabling proper matrix manipulation and image generation.

The libs_par2 routine, developed by the GAIA research group,[23] was used to extract relevant spectral parameters from each spectrum, including (*i*) signal-to-background ratio, (*ii*) total signal area (sum of all peaks in a given interval), and (*iii*) maximum peak intensity. Specific emission lines for each element (Ag, Au, Cu, Sn) were selected based on their relative intensity and absence of spectral interference, as confirmed by Aurora software and summarized in Table 1.

Each set of 720 spectra (12 × 12 grid × 5 pulses *per* point) was compiled into a matrix **M** (720 × E), where E is the number of selected emission lines *per* element. These matrices were normalized by the relative intensity of each emission line to improve the correlation between signal magnitude and concentration. Next, matrices from each leaching step were combined into a single $\mathbf{M}_{\text{combined}}$ matrix (2880 × E), encompassing the original sample size (12 × 12), 5 pulse *per* point and the four sequentially leached residues (12 × 12 × 5 × 4 = 2880).

Data were auto-scaled and submitted to PCA to reduce dimensionality and highlight variance patterns (correlations) related to metal concentrations. PCA scores were then reshaped into 12 × 12 matrices to reconstruct score maps for each element. These images were used to visually assess the spatial distribution and depletion of elements throughout the leaching process. In addition, this type of visualization related to computer vision improves the identification of patterns among the different extractors, and correlation among target metals.

Results and Discussion

Reference concentration obtained by ICP OES

After sequential leaching and sample preparation, as shown in Figure 1, the initial concentrations of the target elements were determined by ICP OES as: Ag at 1,225 mg kg^{-1}, Au at 196 mg kg^{-1}, Cu at 19% m m^{-1} and Sn at 4.5% m m^{-1}. These values can vary significantly depending on the type of e-waste. For example, the average concentration of Cu is 16% in computers and 22% m m^{-1}

Table 1. Emission lines selected for the calculations of maps of scores for the elements Ag, Au, Cu and Sn

Emission line (relative intensity) / nm							
Ag		Au		Cu		Sn	
λ1	224.643 (123)	λ1	204.454 (703)	λ1	213.598 (6104)	λ1	224.605 (2545)
λ2	228.003 (281)	λ2	211.068 (2384)	λ2	224.261 (7634)	λ2	231.723 (1218)
λ3	546.550 (643)	λ3	212.529 (1078)	λ3	224.700 (8046)	λ3	249.570 (1197)
		λ4	443.511 (231)	λ4	324.754 (16256)	λ4	257.158 (1385)
		λ5	460.751 (341)	λ5	327.396 (15301)	λ5	266.124 (1110)
		λ6	481.160 (390)	λ6	515.324 (8297)	λ6	277.981 (1224)
				λ7	521.820 (12349)	λ7	285.062 (2110)
						λ8	452.474 (2741)
						λ9	579.918 (1008)

in cell phones, while that of Au is 430 mg kg^{-1} in cell phones and 390 mg kg^{-1} in computers.[34-37] This variation in concentrations, which depends on both the type of e-waste and the date of manufacture, is a crucial factor in optimizing recovery processes. Knowing these differences allows extraction methods to be adjusted to improve efficiency in the recovery of precious and industrial metals present in e-waste.

Figure 1 shows the leaching sequence applied to the e-waste after the first leach with HNO_3. The remaining leaching tests were designed with the aim of achieving the best conditions for extracting Ag, Au and Sn, maximizing the efficiency of the process. The subsequent leaches tested were carefully planned to improve the synergy between the different leaches used, taking advantage of their complementary characteristics. In addition, the process was structured to minimize possible adverse effects, such as the dissolution of unwanted elements or matrix interference. This approach allows for more precise control of the process and contributes to selective and efficient extraction of the elements of interest.

The results of the leaching tests are shown in Figure 2, where is possible to see the performance obtained in each sequential step.

In Figure 2a, for instance, the HNO_3 lixiviant showed an extraction efficiency of approximately 97% for Cu, 53% for Ag and 79% for Sn, while it was not effective for Au, as this element is not efficiently leached in an acidic medium containing only HNO_3. The leaching sequence in Figures 2b and 2c shows that the simultaneous extractions of Ag and Au were satisfactory, demonstrating significant efficiency for these elements. However, when compared to the stages illustrated in Figures 2d and 2e, it can be seen that the latter were more efficient. This is probably because, in the initial stages, the majority metals, such as Cu and Sn, were extracted first, which influenced the efficiency of the subsequent stages for the minority metals, such as Ag and Au.

Based on the results presented, we can conclude that the most efficient and environmentally friendly sequence was the one illustrated in Figure 2d. In this step, an extraction efficiency of 100% was achieved for Cu and Ag, 97% for Sn

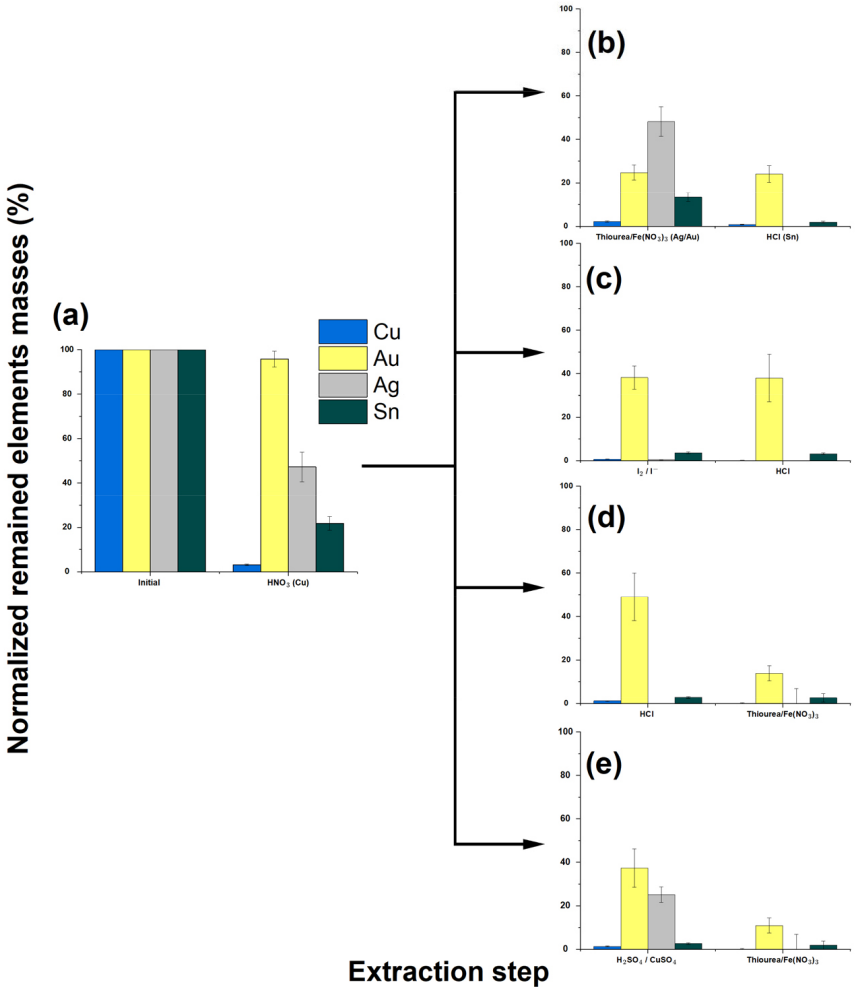

Figure 2. Comparison of the normalized concentrations of sequential leaching obtained by ICP OES: (a) Cu extraction, (b up to e) Ag, Au and Sn extraction with thiourea and $Fe(NO_3)_3$ (for Ag and Au), HCl (for Sn), iodine (I_2)/iodide (I^-) (for Ag and Au), and H_2SO_4 and $CuSO_4$ (for Sn).

and 86% for Au. These results highlight the importance of proper sequence planning to maximize extraction efficiency and minimize the environmental impacts associated with the process.

LIBS as an alternative process control in e-waste recycling

The goal was to evaluate whether the LIBS technique, combined with hyperspectral imaging, could serve as a less expensive alternative to the ICP OES technique for monitoring the consecutive leaching processes of waste-waste. Comparative studies were carried out, as ICP OES is often used in this type of analysis. For this evaluation, the solid waste obtained from the leaching stages shown in Figure 1 was used. The solid material remaining from each experiment was analyzed using the LIBS technique, making it possible to identify the target elements directly on the surface of the samples. This approach sought to verify the effectiveness of LIBS as a fast and cost-effective analysis tool for monitoring selective leaching processes.

Evaluating the LIBS spectra

To carry out the analysis, all the procedures required for pellet formation were followed, without the use of binders, as shown in Figure S2 (SI section). The aim was to assess whether the LIBS technique is robust enough to detect variations in the concentrations of the target elements. To do this, the average emission spectra of the first leaching sequence was analyzed (Figure 1a). Figure 3 shows the spectral regions corresponding to each target element.

In Figure 3a, it can be seen that the Ag emission line signal at 224.64 nm decreases progressively with each leaching step, with the intensity dropping from approximately 3000 a.u. to 10 a.u. This same behavior was identified for Au (Figure 3b), Cu (Figure 3c), and Sn (Figure 3d). They all showed high initial intensities, which progressively decreased to almost zero values at the end of the leaching processes. For example, the Cu emission line at 521.82 nm (Figure 3c), the majority element in the sample, showed a reduction in intensity from 10,000 a.u. to values close to zero. Gold, whose emission line at 443.51 nm (Figure 3b) was monitored, had its intensity reduced from 670 to 21 a.u.

These results show that the LIBS technique has sufficient sensitivity to detect significant changes in the concentration of elements, both for those present in high concentrations, such as Cu and for minority elements, such as Ag and Au. This highlights the potential of LIBS as an effective tool for monitoring concentration variations in electronic waste-leaching processes.

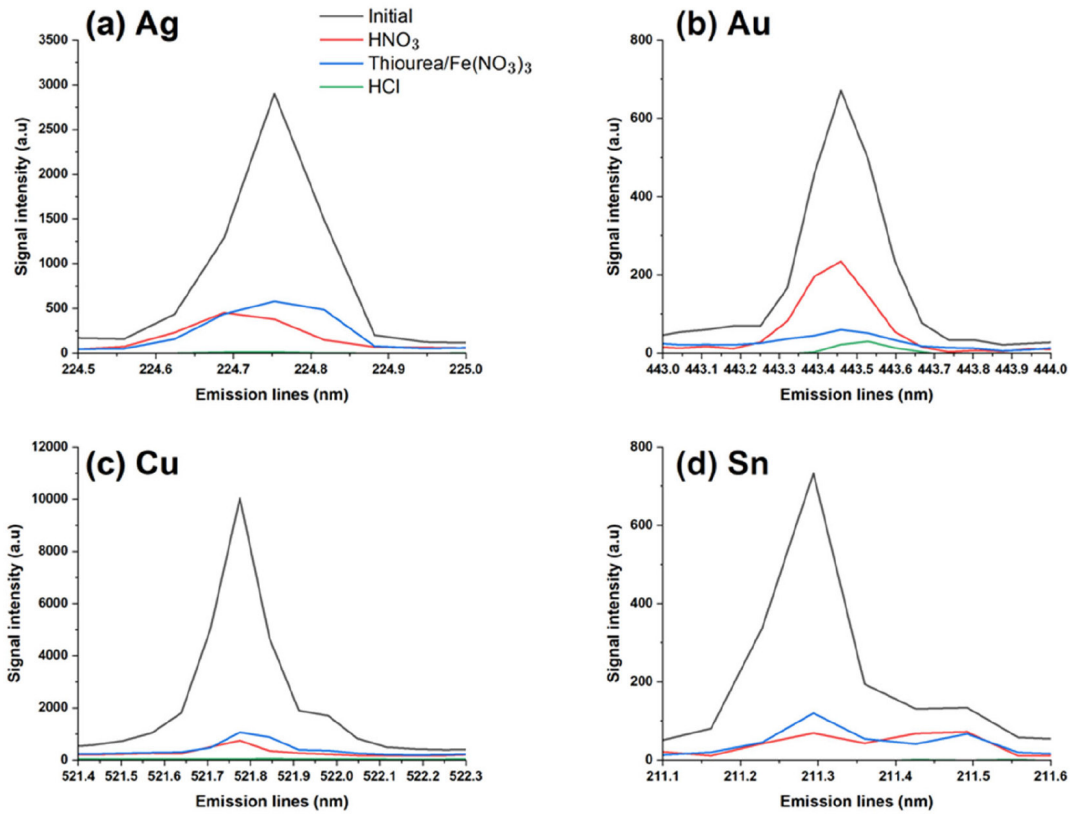

Figure 3. Average emission spectra (arbitrary units) for a sample leached in 3 stages (HNO_3, thiourea, and HCl), considering the emission range of the target elements.

Hyperspectral image interpretation and analysis

After evaluating the average LIBS spectra in the previous section, the most suitable emission lines were selected, avoiding spectral interferences and self-absorption effects, using the Aurora software (Applied Spectra) and the LIBS_par2 routine. The selected lines are shown in Table 1. Based on these lines, the areas of the emission peaks were calculated using the LIBS_par2 routine, generating an **M** matrix of dimension 720 × **E** for each sample in the different leaching stages, where **E** represents the area of each emission line of the target elements. To minimize matrix effects and enable a visual inspection of the quantitative element profiles after each leaching step, the matrix was normalized using relative intensity of each selected emission line (see also Table 1).

With the matrix normalized, the areas corresponding to each leaching step were combined, resulting in the $\mathbf{M}_{\text{combined}}$ matrix, with a dimension of 2880 × **E**. The combination was structured so that each set of 720 spectra represented a leaching stage, in other words, the first 720 × **E** corresponds to the original sample, the spectra from 721 to 1440 × **E** to the sample leached with HNO_3, and so on (see sequence in Figure 1). These combined matrices were generated for each target element and leaching strategy evaluated in this study (Figure 1).

After auto-scaling the data, a PCA was performed for each set of 5 pulses to map the pellet surfaces, and the score values obtained were organized to build a map of scores representing the distribution of elements on the pellet surface after each leaching step.

Figure 4 shows the results obtained for each leaching stage (y-axis) and the respective elements determined. The aim of the hyperspectral images is to visually illustrate the progressive reduction in the signals of the elements at each stage of the process, since, as the elements are extracted, they migrate to the liquid phase, resulting in a lower signal in the solid phase, as observed in the images.

Analysis of the map of scores of the first leaching strategy (Figure 4a) shows that, in the initial phase, all the elements are 100% in the solid fraction, with score values ranging from 4 to 15 (colors from dark green to red). After leaching with HNO_3, aimed at extracting Cu, there is a drop in the Ag, Cu, and Sn signals, while Au remains partially unchanged, since the reaction does not favor its extraction.

A comparison between the maps of scores and the extraction percentages obtained by ICP OES confirms the consistency of the results. For example, Cu, which had an initial average score of 4.29, fell to –0.52 after the last HCl leaching stage. In the case of Ag, during the stages with HNO_3 and thiourea/$Fe(NO_3)_3$, its concentration in the solid phase remained almost constant (47 to 48%), which was reflected in the LIBS spectra, with average scores of 2.0 and 1.8, respectively. This behavior was also observed for the other elements, reinforcing the ability of LIBS associated with hyperspectral images to monitor the extraction of metals throughout the process.

The reliability of this approach is reinforced by the explained variance of calculated PC1 in Figure 4a, which was 99.44% for Ag, 76.78% for Au, 92.43% for Cu, and 83.48% for Sn.

Further evidence of the effectiveness of LIBS can be seen in Figure 4b, where the Au signals in the leaching steps with I_2/I^- and HCl show very similar concentrations. This similarity is also reflected in the map of scores, with average values of 0.26 and 0.24, respectively. The same behavior is visible for Sn (Figure 4c), whose initial concentration of 100% in the solid fraction progressively decreased to 21.7% after leaching with HNO_3, 2.7% after HCl and 2.6% after thiourea/$Fe(NO_3)_3$. This decrease is evident in the hyperspectral image and in the reduction in average scores values, which went from 6.3 in the initial sample to –0.07, –1.19 and –0.98 at the end of the process.

For Ag (Figure 4d), a progressive decrease in the signal is also observed, with average scores reducing from 2.55 (100% in the solid) to 2.06 (47.2% in the solid) after leaching with HNO_3, 0.74 (25.1% in the solid) after $H_2SO_4/CuSO_4$ and –0.65 (0% in the solid) after leaching with HCl. These results show that LIBS is sensitive enough to detect variations in concentration, even at very low levels, such as the reduction in Sn from 21.7 to 2.6% after leaching with thiourea/$Fe(NO_3)_3$.

The central question is: would it be possible to use only LIBS to assess the efficiency of each leaching stage, without ICP OES concentration data? Analysis of the hyperspectral images and average scores indicates that it is, as there are clear differences between each stage.

Considering the average scores in the last leaching stage, the most efficient strategy was the one shown in Figure 4d, with values of –0.59 for Ag, –0.68 for Au, –1.02 for Cu and –1.68 for Sn, resulting in an overall average score of –0.99 (average of the scores for the four elements). The sequence shown in Figure 4c was the second most efficient (overall average score of –0.74), followed by the strategies in Figure 4a (–0.69) and 6b (–0.38).

This result confirms the analysis carried out using ICP OES, which also indicated that the best strategy is the sequential leaching of Cu with HNO_3, Sn with HCl and Ag/Au with thiourea/$Fe(NO_3)_3$, both from the point of view of efficiency and environmental impact. Therefore, despite its limitations, LIBS showed good results in this

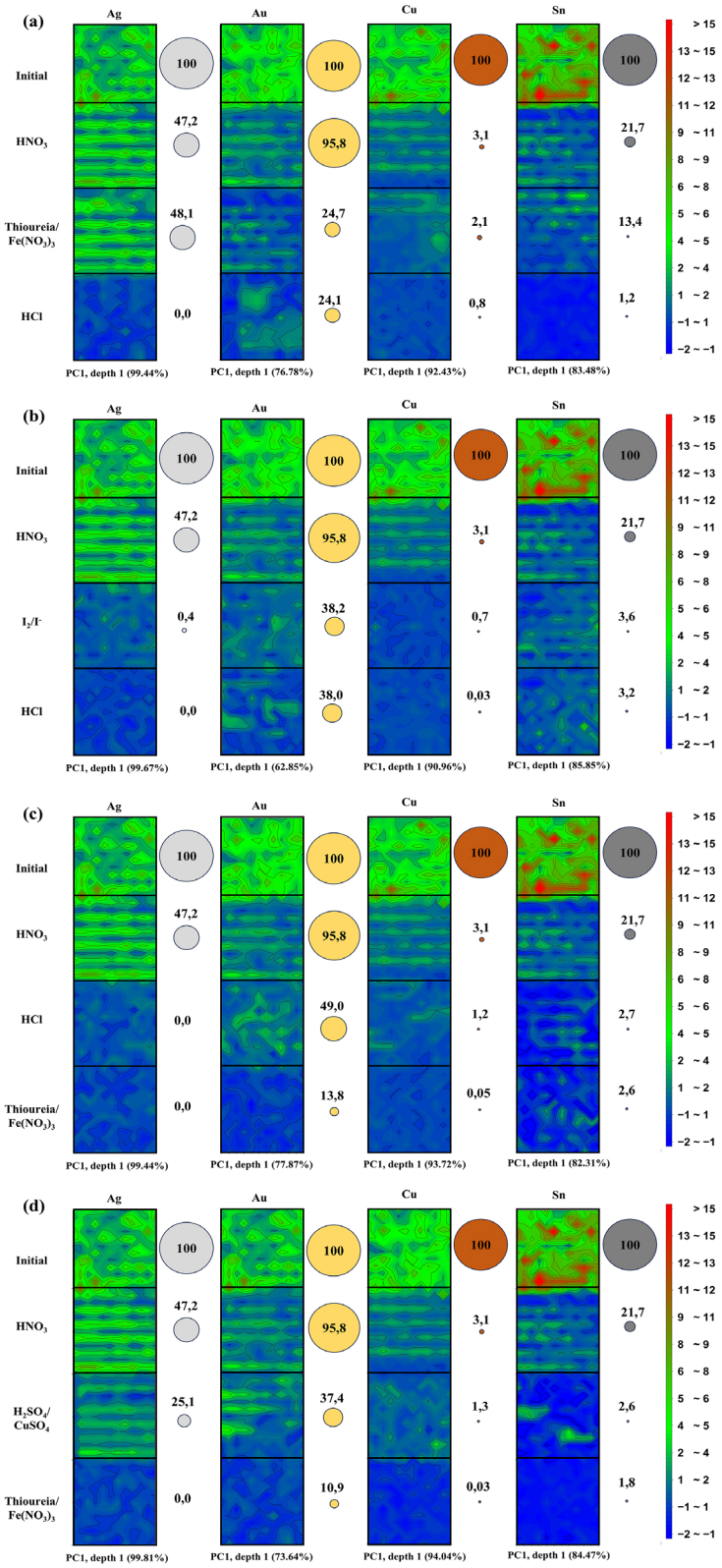

Figure 4. Hyperspectral images generated from PCA scores for the target elements (Ag, Au, Cu, and Sn) after each step of different sequential leaching strategies. Each panel (a-d) represents a unique leaching sequence: (a) leaching with HNO_3, followed by thiourea/$Fe(NO_3)_3$, and finally HCl; (b) leaching with HNO_3, followed by I_2/I^-, and finally HCl; (c) leaching with HNO_3, followed by HCl, and finally thiourea/$Fe(NO_3)_3$; and (d) leaching with HNO_3, followed by $H_2SO_4/CuSO_4$, and finally thiourea/$Fe(NO_3)_3$. The color scale on the right represents the normalized score values, where red tones indicate higher elemental concentration in the solid phase and blue tones indicate lower concentration. The circles next to each score show the percentage of each element remaining in the solid waste after this stage, as determined by ICP OES.

application, demonstrating its potential as an alternative for monitoring e-waste leaching processes.

To correctly interpret these results, it is crucial to clarify the relationship between the static image of the pellet and the dynamic leaching process. As described in the method, the metal extraction is performed with the e-waste powder in suspension. For each monitoring step, a representative aliquot of this powder (inert material) is collected, dried, and pressed into a new pellet for LIBS analysis. The pellet itself, therefore, is not leached, serving as a sampling device that presents a flat, representative surface of the system's solid state for the analysis.

An important consideration is whether the hyperspectral imaging component is fundamental to the monitoring process, or if the average signal from all 720 pulses would be sufficient. While the average LIBS spectra (as shown in Figure 3) are indeed capable of indicating the overall depletion trend of the target elements, relying solely on this integrated signal can be misleading and masks crucial information regarding process efficiency. The primary justification for the imaging approach lies in the inherent heterogeneity of the solid sample, which was quantitatively confirmed by the high initial relative standard deviations (RSD) values (up to 26.8%) reported in Table 2. An average signal could decrease to an acceptable level even if the leaching is occurring non-uniformly, for instance, being highly efficient in some areas of the pellet while completely stalled in others due to poor mixing or surface passivation.

The hyperspectral maps, however, provide essential spatial and diagnostic information, working together with computational vision. They allow for a visual assessment of the uniformity of the reaction, confirming that the metal decrease is occurring across the entire surface and not just in isolated hotspots. This approach can be also implemented in a conveyor belt for real time monitoring of the solid residue after leaching. Therefore, while the average signal can answer if the overall concentration is decreasing, the hyperspectral image is fundamental to understanding how this decrease is happening, providing a much deeper and more reliable level of process control.

Comparative analysis of error and analytical performance of the alternative method

To evaluate the proposed alternative method, a comparative analysis was conducted to assess the analytical errors associated with the LIBS monitoring technique and the ICP OES reference method. The ICP OES served as a reference for quantitative validation, providing accurate reference values for the mass concentration of the elements after sample digestion. This technique is characterized by high precision, with RSD typically between 1 and 5% for homogeneous liquid samples, and very low limits of detection, which were determined in the mg kg^{-1} range for the target elements.

For the LIBS method, precision was assessed to validate the data acquisition strategy, which involved averaging 5 sequential pulses at each of the 144 analytical points. To investigate the characteristics of the sample in detail, a pulse-by-pulse analysis of the precision was conducted by calculating the RSD for each individual pulse across the 144-point grid of the initial, non-leached sample. The results are presented in Table 2.

The data in Table 2 reveal an aspect of this complex material. Unlike homogeneous samples where the RSD typically decreases significantly after the first pulse due to surface cleaning, the RSD for the e-waste sample remains consistently high across all five pulses. For instance, the RSD for Cu, the major element, fluctuates in the high range of 46-53% without a clear downward trend. A similar behavior is observed for the other elements. This sustained high variance is attributed to the extreme micro-heterogeneity of the sample. The pressed pellet is a composite of distinct metallic and polymeric particles. Within a single 100 μm analysis spot, the five sequential laser pulses are not ablating a uniform surface, but are likely drilling through different materials (for example, a

Table 2. Pulse-to-pulse analysis of the RSD calculated from the 144-point grid for the initial (non-leached) sample

Laser pulse	RSD / %			
	Ag (224.64 nm)	Au (211.06 nm)	Cu (521.82 nm)	Sn (303.41 nm)
1st pulse	45.65	28.37	50.50	29.08
2nd pulse	45.75	27.84	53.06	27.86
3rd pulse	48.73	28.78	51.89	28.56
4th pulse	42.24	28.70	50.95	30.99
5th pulse	46.56	29.80	46.54	30.23
5-pulse average	45.79	28.70	50.59	29.34

RSD: relative standard deviation.

Table 3. Pulse-to-pulse analysis of the RSD for the sample after the final leaching step of sequence Figure 4c

Laser pulse	RSD / %			
	Ag (224.64 nm)	Au (211.06 nm)	Cu (521.82 nm)	Sn (303.41 nm)
1st pulse	83.37	71.86	78.67	60.48
2nd pulse	88.91	62.17	87.03	55.48
3rd pulse	69.34	66.28	78.97	58.28
4th pulse	86.44	70.10	82.16	53.52
5th pulse	86.55	71.51	72.82	62.35
5-pulse average	82.92	67.51	79.93	58.02

RSD: relative standard deviation.

Cu fragment, then a polymer particle), causing significant pulse-to-pulse signal fluctuation.

To further investigate how the leaching process affects this heterogeneity, the same pulse-by-pulse analysis was performed on the solid residue after the final leaching step of sequence Figure 4c. The results are presented in Table 3.

A direct comparison between the data from the initial sample (Table 2) and the final leached sample (Table 3) reveals a significant increase in RSD. This trend is characteristic of measurements approaching the limit of detection in heterogeneous materials and confirms efficient extraction. After leaching, only sparse and isolated metal fragments remain. The analysis results in a signal distribution with many low values and a few high-intensity peaks, which mathematically leads to a very high RSD. Therefore, this increase in RSD serves as a quantitative indicator of the effectiveness of leaching.

With the 5-pulse average method validated as essential for this type of sample, Table 4 summarizes the resulting average RSD for each complete leaching step across all strategies. This table allows for an evaluation of the overall spatial heterogeneity at each stage of the process.

The RSD values for the initial non-leached sample were significantly high (e.g., 23.1% for Ag and 22.9% for Cu), as shown in Table 4. This quantitatively confirms the considerable spatial heterogeneity of the metal distribution on the pellet surface, a key finding that validates the use of a spatially resolved technique such as hyperspectral imaging rather than simple point-and-shoot analysis. Interestingly, the RSD for certain elements increased during the intermediate leaching stages (Cu to 40.3% after leaching with HNO_3), indicating that the leaching process itself occurs unevenly, temporarily increasing the relative heterogeneity of the remaining metal. In addition, the extremely high RSD values in the final leaching stage (> 100% for Ag) are characteristic of signals approaching the limit of detection of the method. This does not indicate low precision, but confirms a highly efficient extraction, where the residual signal is comparable to instrumental noise.

Table 4. RSD calculated from the LIBS signal intensity for each leaching step of the sequences described in Figure 4

Leaching step	RSD / %			
	Ag	Au	Cu	Sn
Sequence (Figure 4a)				
Initial	23.1	22.2	22.9	11.8
HNO_3	12.3	40.3	31.2	11.7
Thiourea/$Fe(NO_3)_3$	66.7	64.4	56.6	59.3
HCl	146.2	12.2	18.3	13.1
Sequence (Figure 4b)				
Initial	23.1	22.2	21.3	26.8
HNO_3	12.3	40.3	21.8	6.3
I_2/I^-	78.8	17.7	19.2	14.3
HCl	47.6	10.9	8.7	8.3
Sequence (Figure 4c)				
Initial	23.1	22.2	21.3	26.8
HNO_3	12.3	40.3	21.8	6.3
HCl	63.3	12.3	13.8	51.7
Thiourea/$Fe(NO_3)_3$	164.9	11.7	10.8	13.4
Sequence (Figure 4d)				
Initial	23.1	22.2	21.3	11.8
HNO_3	12.3	40.3	21.8	11.7
$H_2SO_4/CuSO_4$	129.3	11.8	11.1	15.6
Thiourea/$Fe(NO_3)_3$	19.0	10.9	9.5	12.6

Data obtained from analysis of emission lines: Ag (224.643 nm), Au (211.068 nm), Cu (521.82 nm), Sn (303.412 nm).

Conclusions

This study demonstrated the application of the LIBS technique associated with hyperspectral images as an alternative for controlling metal leaching processes in e-waste. The optimized leaching strategy, validated by ICP OES, proved highly efficient, achieving extraction rates of 100% for Cu and Ag, 97% for Sn, and 86% for Au. The LIBS data showed excellent correlation with these findings; the progressive reduction in spectral signals was compatible with the extraction efficiencies, with the signal

from the majority element, Cu, being reduced to near-zero values by the end of the process.

These results show that the LIBS technique is promising for monitoring e-waste recycling processes, providing a faster and more economical alternative to ICP OES. The claim that this approach is more economical than conventional monitoring via ICP OES is based on two fronts. Firstly, on direct analytical costs: the LIBS method eliminates the need for expensive consumables, such as the high-purity argon gas required by ICP OES, and dispenses with the time-consuming acid digestion step, which requires reagents and specialized labor. Secondly, and more importantly, the economic advantage lies in implementing LIBS as a process analytical technology. The ability to obtain real-time data on leaching efficiency allows for dynamic process control, making it possible to stop the reaction at the optimal moment. This translates into a significant reduction in the consumption of leaching reagents and energy, in addition to increasing plant throughput economic benefits on an industrial scale that far outweigh the cost of the analysis itself.

However, future studies could focus on improving chemometric models to optimize the element quantification process and minimize matrix interference. In addition, the application of LIBS on an industrial scale can contribute significantly to optimizing metal recovery, strengthening the circular economy and reducing the environmental impacts associated with the inappropriate disposal of e-waste.

Supplementary Information

Supplementary information is available free of charge at http://jbcs.sbq.org.br as PDF file.

Data Availability Statement

We declare that all the experimental data in this paper are obtained through experimental tests and have absolute authenticity. All relevant data are within the paper.

Acknowledgments

This study was financed, in part, by the São Paulo Research Foundation (FAPESP), Brazil, Process No. 2019/24223-5. The authors are also grateful to National Council for Scientific and Technological Development, CNPq (grants No. 140867/2021-0, 302719/2020-2, and 304684/2024-4). This study was partly funded by the Coordination for the Improvement of Higher Education Personnel - Brazil (CAPES) - Funding Code 001.

Author Contributions

Dennis S. Ferreira was responsible for writing original draft, visualization, validation, methodology, investigation and Edenir R. Pereira-Filho for supervision, resources, project administration, funding acquisition, formal analysis, data curation.

References

1. Patil, R. A.; Ramakrishna, S.; *Environ. Sci. Pollut. Res.* **2020**, *27*, 14412. [Crossref]
2. Zhang, L.; Qu, J.; Sheng, H.; Yang, J.; Wu, H.; Yuan, Z.; *Resour. Conserv. Recycl.* **2019**, *143*, 210. [Crossref]
3. Baldé, C. P.; Kuehr, R.; Yamamoto, T.; McDonald, R.; Althaf, S.; Bel, G.; Deubzer, O.; Fernandez-Cubillo, E.; Forti, V.; Gray, V.; Herat, S.; Honda, S.; Iattoni, G.; Khetriwal, D. S.; Luda, V. C.; *The Global E-waste Monitor 2024*; ITU and UNITAR: Geneva, Bonn, 2024.
4. Parajuly, K.; Kuehr, R.; Awasthi, A.; Fitzpatrick, C.; Lepawsky, J.; Smith, E.; Widmer, R.; Zeng, X.; *Future E-waste Scenarios*; UNU/UNEP: Bonn, Osaka, 2019.
5. Forti, V.; Baldé, C. P.; Kuehr, R.; Bel, G.; *The Global E-waste Monitor 2020: Quantities, Flows and the Circular Economy Potential*; UNU/UNITAR, ITU and ISWA: Bonn, Geneva, Rotterdam, 2020.
6. Sengupta, D.; Ilankoon, I. M. S. K.; Kang, K. D.; Chong, M. N.; *Miner. Eng.* **2023**, *200*, 108154. [Crossref]
7. Stockholm Convention on Persistent Organic Pollutants (POPs); *The Convention - Overview*; http://www.pops.int/TheConvention/Overview/tabid/3351/Default.aspx, accessed in August 2025.
8. United Nations Industrial Development Organization (UNIDO); https://www.unido.org/our-focus/safeguarding-environment/implementation-multilateral-environmental-agreements/stockholm-convention, accessed in August 2025.
9. Dutta, D.; Rautela, R.; Gujjala, L. K. S.; Kundu, D.; Sharma, P.; Tembhare, M.; Kumar, S.; *Sci. Total Environ.* **2023**, *859*, 160391. [Crossref]
10. Xavier, L. H.; Ottoni, M.; Abreu, L. P. P.; *Resour. Conserv. Recycl.* **2023**, *190*, 106840. [Crossref]
11. Dobó, Z.; Dinh, T.; Kulcsár, T.; *Energy Rep.* **2023**, *9*, 6362. [Crossref]
12. Li, X. G.; Gao, Q.; Jiang, S. Q.; Nie, C. C.; Zhu, X. N.; Jiao, T. T.; *J. Environ. Manage.* **2023**, *348*, 119288. [Crossref]
13. Ferreira, D. S.; Pereira-Filho, E. R.; *Hydrometallurgy* **2025**, *235*, 106476. [Crossref]
14. Tembhare, S. P.; Bhanvase, B. A.; Barai, D. P.; Dhoble, S. J.; *Environ. Develop. Sustainable* **2022**, *24*, 8965. [Crossref]
15. Mishra, K.; Siwal, S. S.; Thakur, V. K.; *Curr. Opin. Green Sustainable Chem.* **2024**, *47*, 100900. [Crossref]
16. Debnath, B.; Chowdhury, R.; Ghosh, S. K.; *Front. Environ. Sci. Eng.* **2018**, *12*, 2. [Crossref]

17. Muscetta, M.; *Chem. Eng. Process.* **2024**, *204*, 109937. [Crossref]
18. Binnemans, K.; Jones, P. T.; *J. Sustainable Metall.* **2022**, *9*, 1. [Crossref]
19. Limbeck, A.; Bonta, M.; Nischkauer, W.; *J. Anal. At. Spectrom.* **2017**, *32*, 212. [Crossref]
20. Desroches, D.; Bédard, L. P.; Lemieux, S.; Esbensen, K. H.; *Miner. Eng.* **2018**, *126*, 36. [Crossref]
21. Castro, J. P.; Machado, R. C.; Andrade, D. F.; de Babos, D. V.; Pereira-Filho, E. R.; Garcia, J. A.; Sperança, M. A.; Gamela, R. R.; Costa, V. C.; *Quantitative Analysis*, 1st ed.; Springer International Publishing: Cham, 2017.
22. Brunnbauer, L.; Gajarska, Z.; Lohninger, H.; Limbeck, A.; *TrAC, Trends Anal. Chem.* **2023**, *159*, 116859. [Crossref]
23. Pereira-Filho, E. R.; *Laser-Induced Breakdown Spectroscopy (LIBS): Applications and Calibration Strategies*; Editora Ibero-Americana de Educação: São Carlos, 2021.
24. Noll, R.; Sturm, V.; Aydin, Ü.; Eilers, D.; Gehlen, C.; Höhne, M.; Lamott, A.; Makowe, J.; Vrenegor, J.; *Spectrochim. Acta, Part B* **2008**, *63*, 1159. [Crossref]
25. Myakalwar, A. K.; Sandoval, C.; Velásquez, M.; Sbarbaro, D.; Sepúlveda, B.; Yáñez, J.; *Minerals* **2021**, *11*, 1073. [Crossref]
26. International Union of Pure and Applied Chemistry (IUPAC); *Spectrochim. Acta, Part B* **1978**, *33*, 241. [Crossref]
27. Ferreira, D. S.; Pereira, F. M. V.; Olivieri, A. C.; Pereira-Filho, E. R.; *Anal. Chim. Acta* **2024**, *1303*, 342522. [Crossref]
28. Dutta, D.; Panda, R.; Kumari, A.; Goel, S.; Jha, M. K.; *Sustainable Mater. Technol.* **2018**, *17*, e00066. [Crossref]
29. Behnamfard, A.; Salarirad, M. M.; Veglio, F.; *Waste Manage.* **2013**, *33*, 2354. [Crossref]
30. Xiu, F. R.; Qi, Y.; Zhang, F. S.; *Waste Manage.* **2015**, *41*, 134. [Crossref]
31. Moosakazemi, F.; Ghassa, S.; Mohammadi, M. R. T.; *J. Cleaner Prod.* **2019**, *228*, 185. [Crossref]
32. Guo, X.; Qin, H.; Tian, Q.; Li, D.; *J. Hazard. Mater.* **2020**, *384*, 121355. [Crossref]
33. Ferreira, D. S.; Rodrigues, L. S.; Pereira, F. M. V.; Pereira-Filho, E. R.; *Quim. Nova* **2023**, *46*, 747. [Crossref]
34. Lu, Y.; Xu, Z.; *Resour., Conserv. Recycl.* **2016**, *113*, 28. [Crossref]
35. Chen, M.; Wang, J.; Chen, H.; Ogunseitan, O. A.; Zhang, M.; Zang, H.; Hu, J.; *Environ. Sci. Technol.* **2013**, *47*, 12409. [Crossref]
36. Jing-ying, L.; Xiu-li, X.; Wen-quan, L.; *Waste Manage.* **2012**, *32*, 1209. [Crossref]
37. Sheng, P. P.; Etsell, T. H.; *Waste Manage. Res.* **2007**, *25*, 380. [Crossref]

Submitted: June 16, 2025
Final version online: August 20, 2025